

Correlation between optical and shielding properties of phosphate glasses with alkaline oxide and their application

K. I. Hussein^{a,b,c}, M. S. Alqahtani^{a,b}, A. Almarhaby^d, R. S. Alayyash^{b,*}, E. Elshiekh^b

^aResearch Center for Advanced Materials Science (RCAMS), King Khalid University, Postcode: 9004, Zip code: 61413, Abha, Saudi Arabia

^bDepartment of Radiological Sciences, College of Applied Medical Sciences, King Khalid University, Abha 61421, Saudi Arabia

^cDepartment of Medical Physics and Instrumentation, National Cancer Institute, University of Gezira, Wad Medani 2667, Sudan

^dMedical Physics Department, King Fahd General Hospital, Ministry of Health, Al Andalus, Jeddah 23325, Jeddah

In numerous tissue engineering and dental applications, bioactive glasses are utilized. These glasses have unique characteristics that make them attractive candidates for a variety of applications. A new bioactive glass system with the structure of $45\text{P}_2\text{O}_5 - 20\text{CaO} - 15\text{CaCl}_2 - 8\text{KF} - (10 - x)\text{Li}_2\text{O} - (x)\text{TiO}_2$ was developed in this study, with $x = 2, 6, \text{ and } 8$ mol%. For usage in radiation protective applications, it was evaluated. By using an ultraviolet-visible spectrophotometer, we were able to measure the absorbance (Abs) and transmittance (T %) in the range of wavelengths 190–2500 nm. Furthermore, the optical energy gap of the produced glasses was determined. Using the MIKE software, the mass attenuation coefficients (MAC) of the bioactive glasses under investigation were calculated for energies ranging from 15 to 200 keV. The $LAC, Z_{eff}, N_{eff}, HVL, TVL, \text{ and } MFP$ (Linear attenuation coefficient, effective atomic number, effective electron density, half value layer, tenth value layer, and mean free path) of the bioactive glasses were calculated. According to the findings, the addition of titanium dioxide (TiO_2) as well as the metal oxide such as Li_2O to bioactive glasses generates significant differences in the attenuation characteristics of bioactive glasses. The results indicate that the PCKLT3 ($\text{TiO}_2 = 8\text{mol}\%$) bioactive-glass sample had the best attenuation among other samples.

(Received November 11, 2022; Accepted March 2, 2023)

Keyword: Phosphate glass, Density, UV- Vis-NIR, Optical energy gap, Mass attenuation coefficient, Half valuer layer

1. Introduction

Bioactive glass systems are formed of amorphous structures containing silicon, calcium, sodium, phosphorous, and oxygen. Theoretical investigations of bioactive glasses and their radiation attenuation capacities add to the current body of knowledge in the field of advanced medical applications when it is difficult or impossible to do practical or clinical trials. Bio-active glass is a cutting-edge material with several applications. Even though it has been around for roughly four decades, only in the last ten years has it become widely available for commercial use [1,2]. A bioactive glass is a substance that reacts with bodily fluids, killing germs, simulating cells, and assisting in tissue repair. Bioactive glasses are also often employed as bone replacements and, more recently, as co-drug delivery systems [3]. The greatest serious danger to people and the environment today is radiation. As a result of the increasing usage of radiation in a variety of areas, developing suitable alternative shielding materials is required. Although lead (Pb) and ordinary concrete are presently thought to be excellent shielding substances, they are extremely costly,

* Corresponding author: ranasaalayash@gmail.com
<https://doi.org/10.15251/JOR.2023.192.141>

poisonous, inefficient for neutron-shielding. To date, a significant amount of work has been put into the development of radiation shielding materials that are inexpensive, non-toxic, practical, and efficient. A number of industrial glasses, types of high-molecular-weight glasses (HMO glasses), concrete, rocks, and alloys have been proposed as potential radiation shielding materials [4–18]. Recently, bioactive glasses doped with various compounds have been proposed for radiation protection applications. [19–22]. Some TiO_2 treated bioactive glasses have recently been found to aid in the replacement and repair of bone tissue [3]. These bioactive glasses' structural, thermal, and mechanical properties were studied. The TiO_2 additive does have a density of 4.26 g/cm^2 and an atomic number (Z) of (22) for the element (Ti) [23]. Such characteristics are desirable and intriguing in the development of a novel shielding material. The goal of this research is to evaluate the photon attenuation characteristics of a newly created bioactive glass system in the chemical form of $45P_2O_5 - 20CaO - 15CaCl_2 - 8KF - (10 - x) Li_2O - (x) TiO_2$, where $x = 2, 6,$ and 8 mol\% , for use in a variety of medical applications. Some parameters, such as the μ/ρ , MFP , and Z_{eff} , may be used to determine the radiation shielding qualities. The $MFP, HVL,$ and Z_{eff} are all related shielding metrics, and the μ/ρ offers basic information on shielding materials.

2. Materials, density, and optical synthesis

The phosphate glasses with the composition $45P_2O_5 - 20CaO - 15CaCl_2 - 8KF - (10 - x) Li_2O - (x) TiO_2$ (Where $x = 2, 4,$ and 6) in Mol percentage were prepared using melt-quenching technique. The raw materials were put in Pt crucible in the heating furnace at a temperature of in range from 1200 to $1250 \text{ }^\circ\text{C}$ for 30 min depend on the composition, the melt was stirred, when the viscous of it was high consequently the melt cast in the brass mold. The prepared sample was put in the annealing furnace for 2 h at $420 \text{ }^\circ\text{C}$ and after that switch off. A helium pycnometer (UltraPyc1200e) was used to measure samples densities. Samples densities and the chemical compositions of the prepared samples together with the computed refractive index (n) are illustrated in Table 1. The optical absorption spectra were measured in wavelength from 200 to 2500 nm range by using a UV–VIS–NIR spectrophotometer (JASCO V-570) spectrophotometer

3. Results and discussion

3.1. Optical properties of prepared glasses

The optical absorption spectra of the manufactured glasses in the wavelength range of 190 – 2500 nm was measured with a resolution of (2 nm) using a single mono-chromator UV Visible-Near Infrared Spectro-photometer. As demonstrated in Figure 1A, absorbance spectra exhibit an appealing trend across a wavelength range of 190 to 2500 nm . There are two ranges for all spectral glasses. All PCKLT spectra exhibit a diminishing trend with increasing incidence wavelength in the wavelength range (190 – 300) nm . On the other hand, in the visible range of wavelengths (500 – 1000) nm , there is a maximum peak at the region of the absorption in the near ultraviolet (UV) spectrum of light, which indicates that the absorption has occurred. These findings indicate that certain pollution was present through the manufacturing procedure. As a result, the PCKLT 6% and 8% absorb the greatest amount of visible light, which is essential for optical applications. A Perkin-Elmer Lambda 900 spectrophotometer was used to record the transmission spectra. Figure.1B. depicts the total transmission spectra of the studied glasses, which range from 190 – 2500 nanometers (ultraviolet (UV) through visible (Vis) to mid infrared (MIR)). The visible-range transmission spectrum of the glass sample revealed that it has excellent transparency. This indicates that the manufactured glasses exhibit excellent transparency to visible light.

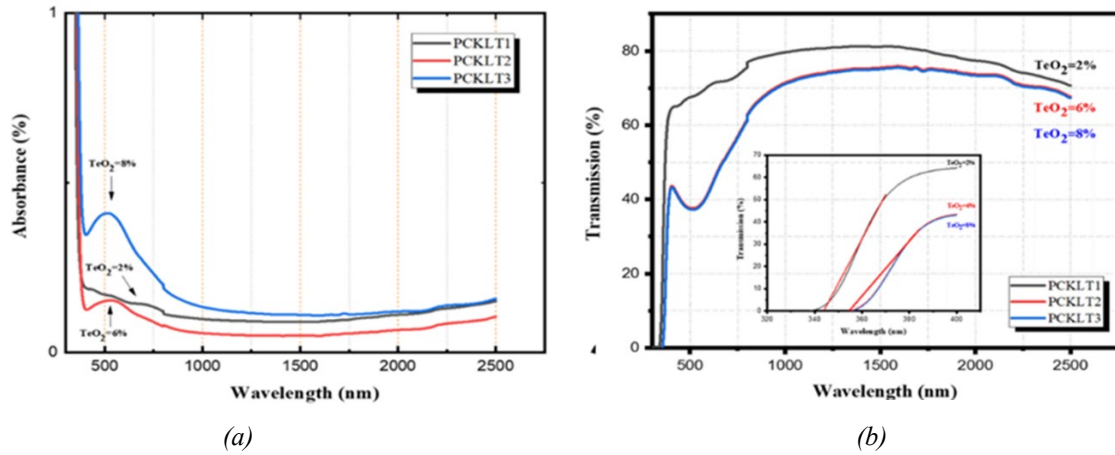


Fig.1. (a) Absorbance spectroscopy of different composition of PCKLT, (b) UV-Vis-NIR transmission spectra of the TiO_2 doped Bioactive glasses.

By submerging glass samples in toluene at room temperature, the density of the glass samples (ρ_{glass}) was determined using Archimedes' method (Equation 1).

$$\rho_{glass} = \frac{W_a}{W_a - W_T} \rho_T \quad (1)$$

where W_a : is the weight of the glass sample in air, W_T : the weight of the glass sample in toluene liquid, and ρ_T : is the density of toluene liquid (0.86 g/cm^3 at room temperature). The measured values of densities of the proposed samples were listed in the following table (Table 1).

Table 1. Chemical compositions of prepared glasses in mol% doped with Tm_2O_3 concentration, density, and refractive Index.

Sample No	Glass composition	Density	Refractive index at (479nm)
PCKLT1	45P ₂ O ₅ -20CaO-15CaCl ₂ -8KF-10Li ₂ O-2TiO ₂	2.6263	2.313
PCKLT2	45P ₂ O ₅ -20CaO-15CaCl ₂ -8KF-10Li ₂ O-6TiO ₂	2.67321	2.327
PCKLT3	45P ₂ O ₅ -20CaO-15CaCl ₂ -8KF-10Li ₂ O-8TiO ₂	2.7451	2.642

The molar volume (V_m), the molar volume of oxygen (V_o), and oxygen packing density, ($O. p. d$) were calculated using the following Equations:

$$V_m = \frac{\sum ix_i m_i}{\rho_{glass}} \quad (2)$$

and,

$$V_o = (V_m) \cdot \left(\frac{1}{x_i n_i} \right) \quad (3)$$

and,

$$O.p.d = \sum i \frac{1000 \cdot \rho \cdot n_i}{m_i} \quad (4)$$

where (x_i) is the molar fraction of each oxide, (m_i) is the molecular weight of the glassy composition, and (n_i) is the number of oxygen atoms in each oxide. When interpreting the density or fragility of the existing glass mesh, all of these variables were considered, and the results are provided in Table 2. When the TiO_2 ions concentration is increased from 2 to 8 mol %, the density rises from 2.623 to 2.7451 $gm.cm^{-3}$ and, *O.p.d.* value decreases from 67.367 to 69.967 $gm.atm.L^{-1}$. On the other hand, V_m and V_o are proportional to the spatial distributions of oxygen in the glass matrix, they are reduced from 38.446 to 37.875 cm^3 and from 14.844 to 14.294 $cm^3.mol^{-1}$ respectively. Factors such as (i) the molecular weight of components in the glass composition, (ii) the amount of oxygen atoms and bond length, (iii) the cation radius, and the coordination number all contribute to changes in V_m and V_o . These factors we must be taken into account for interpretation for the changing in values of V_m and V_o . In prepared glasses, the density value is related to changes in the structure of the glass, and it is influenced by several factors, including the molecular weight of the constitution for the glass composition, coordination numbers with interstitial spaces, and the density of crosslinks in the glass composition. The addition of TiO_2 causes the network of glasses to expand, resulting in an increase in density. When TiO_2 ions are added to the host glasses (PCKLT1) and the V_m value increases, the change in molecular weight is higher than the change in density value. The higher values of the ionic radii and the creation of soluble free ions of TiO_2 in the host glass matrix may be ascribed to the reduction in V_o and rise in *O.p.d.* of the produced glasses. Furthermore, the change in *O.P.D* value with modifier type is in the opposite direction of the change in oxygen molar volume value.

Table 2. The molar volume V_m , oxygen molar volume, V_o , optical packing density, *O.p.d.*, energy gap E_{opt} , Urbach energy, ΔE , of prepared glasses.

Sample code	V_m ($cm^3.mole^{-1}$)	V_o ($cm^3.mole^{-1}$)	O.P.D (mole $^{-1}$)	Energy gap, E_{opt} , in (eV)	Urbach energy, ΔE , in eV
PCKLT1	38.446	14.844	67.367	3.362	0.2964
PCKLT2	38.519	14.646	68.277	3.294	0.2833
PCKLT3	37.875	14.292	69.967	3.236	0.3034

The following formula [24] may be used to calculate the absorption coefficient:

$$\alpha(v) = \frac{1}{d} \ln \left(\frac{I_0}{I_t} \right) = \frac{2.303 \cdot A}{d} \quad (5)$$

where, the incident light frequency denotes (ν), the incident and transmitted beam intensities indicate to (I_0 and I_t), the optical absorbance is (A), the thickness of the glass sample in cm represents (d). It depends on the energy of the photon $h\nu$, such: $\alpha\nu = C \exp(h\nu/E_{opt})$, where, constant is a C , the Urbach energy (ΔE) may be attributed to phonon-assisted indirect electronic transitions and is indicated by the width of the tail of localized states in the energy gap of the band. By calculating (1/slopes) of the linear part of the $\ln \alpha(\nu)$ vs. $h\nu$, to evaluate ΔE , see Figure 2A. We find the maximum value is $\Delta E = 0.3034$ eV for $45P_2O_5 - 20CaO - 15CaCl_2 - 8KF - 4Li_2O - 8TiO_2$, while the lowest value is $\Delta E = 0.2964$ eV for $45P_2O_5 - 20CaO - 15CaCl_2 - 8KF - 10Li_2O - 2TiO_2$. The Urbach sharp edge does not appear, so we suggest that the amorphous phase of the produced glasses is in good accord with data reported for inorganic glasses [14]. It is known that Urbach energy can be considered as a measure of disorder in the glasses. As a result, glass with lower Urbach energies has a reduced chance of bond breakage and defect development. This implies that the glasses under investigation have a good homogenous nature. The following formula [25] may be used to determine the optical band gap:

$$(ah\nu)^n = A(h\nu - E_g) \quad (6)$$

where, (A) is constant, optical band gap is (E_g), the incident spectrum's energy is ($h\nu$) and the absorption coefficient is (α). The value (n) is equal to "2" if a direct transition is allowed. Alternatively, if (n) equals "1/2", it is tied to an indirect transition that is allowed. In this instance, the results indicate that the optimal fit is confirmed for $n = 1/2$. Figure 2B depicts the connection between and for PCKLT-doped glasses with varying titanium concentrations. Therefore, the dominant transition mechanism for PCKLT-doped glasses with varying concentrations is an indirect allowed transition. The value of E_{opt} is in the range 3.236 to 3.362 eV depending on the TiO_2 ions concentration doped the host glasses PCKLT1 (Table 2). It increases from 3.287 to 3.368 eV when increasing TiO_2 from 6 to 8 mol% in the host matrix PCKLT1. The uncertainty of E_{opt} is $\pm 4\%$. The refractive index was determined using an M-2000 Woollam ellipsometer and the refractive index was given in Table 1. It increases from 2.313 to 2.642 with increasing doped TiO_2 ions from 2 to 8 mol%. The refractive index is influenced by a variety of factors, including (i) the coordination number of the doping ions, (ii) the polarizability of the first adjacent ions (anion), (iii) the density of component materials, and (vi) optical basicity of the bulk glasses. The molar refraction (R_m), molar polarizability (α_m) and metallization criterion (M_c) of the prepared samples were obtained by utilizing Eq. (7) (8) (9):

$$R_m = V_m \cdot \left(\frac{n^2 - 1}{n^2 + 1} \right) \quad (7)$$

$$\alpha_m = \frac{3}{4\pi N_A V_m} \cdot \left(\frac{n^2 - 1}{n^2 + 1} \right)^{-1} \quad (8)$$

$$M_c = 1 - \frac{n^2 - 1}{n^2 + 1} \quad (9)$$

where (N_A) is Avogadro's number. The values of (R_m) and (α_m) values are increased from 22.754 to 25.222 in $cm^3 \cdot mol^{-1}$ and from 9.029 to 10.009 in \AA^3 , respectively, with increasing doping TiO_2 from 2 to 8 mol% in the host PCKLT1 glasses, Table (3). The value M_c , decrease from to 0.408 to 0.334 at with increasing doped TiO_2 from 2 to 8 mol% in the host (PCKLT1) glasses.

Table 3. The molar reflection, R_m , electronic polarizability, α_m , , metallization criterion, M_c , of the studied glasses.

Sample code	Molar polarizability, α_m , (\AA^3)	Molar refraction, R_m , (cm^3/mol)	Metallization criterion, M_c ,
PCKLT1	9.029	22.754	0.408
PCKLT2	9.101	22.935	0.405
PCKLT3	10.009	25.222	0.334

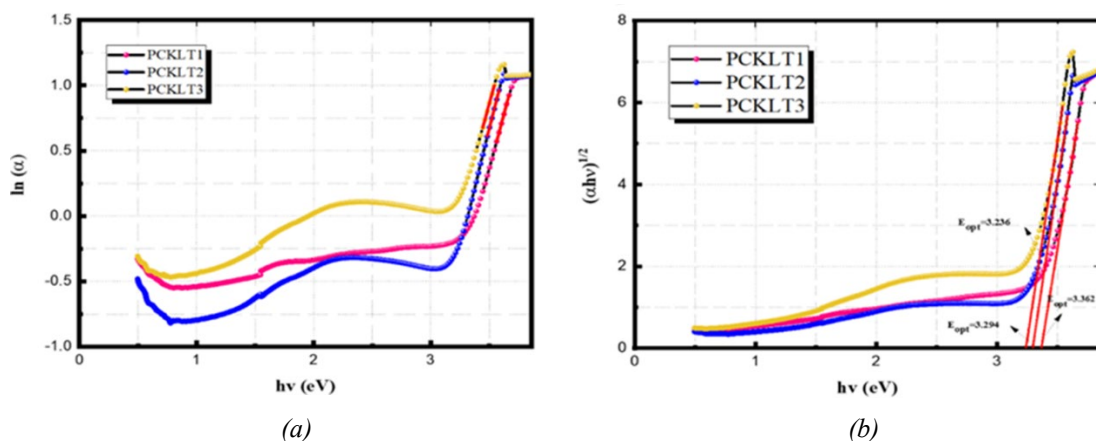


Fig. 2. (a) Plot of $\ln(\alpha)$ with $h\nu$ of glass samples; (b) The dependence of $(\alpha h\nu)^{1/2}$ on the photon energy ($h\nu$) for the prepared glass samples.

2.2. Radiation shielding properties

The Lambert-Beer law was used to calculate the (*LAC* μ) of the selected glasses in the 15–200 keV range, and the resulting values were used to determine the (*MAC* μ/ρ) of the samples.

Pursuant to this law, when a narrow beam of photons with the intensity (I_0) travels through a material with a thickness (x), the intensity that goes through is reduced to a value (I) due to the physical interactions. The following is the formulation of this law [26].

$$I = I_0 e^{-\mu x} \quad (10)$$

$$\mu_{m, glass} = \sum_i w_i (\mu_m)_i \quad (11)$$

In this research paper, Using the MIKE software, different ionizing radiation shielding parameters of Bioactive glasses were estimated for photon energies ranging from 15 to 200 KeV. When calculating specific radiation shielding parameters, it is essential to perform itemized computations in order to fully comprehend the shielding properties of the $P_2O_5 - CaO - CaCl_2 - KF - Li_2O - TiO_2$ glasses. Low-energy photons are more easily shielded by glass than high-energy photons. The meaning of "mass attenuation coefficient, μ/ρ " is an appropriate quantity for obtaining an accurate image of the shielding properties of the produced $P_2O_5 - CaO - CaCl_2 - KF - Li_2O - TiO_2$ glasses. The atomic numbers of the samples examined in this study are close to one other. This result agrees with the literature that the coefficient of linear attenuation varies with the density of the material. The greater the atomic number of high-density glasses, the more likely it is that they will be used as an X-ray shielding material in the future. The (μ/ρ) value of Bioactive glasses is also dependent on the chemical composition of the glasses. The obtained findings are changed in accordance with MIKE. The (*MAC* μ/ρ) values for a matter are based on (i) photoelectric absorption, (ii) Compton scattering, and (iii) pair production. Figure 3A illustrates the values for three distinct bioactive glasses at various energies ranging from 15 to 200 keV. The greatest and lowest photon interaction parameter (μ/ρ) values were achieved with PCKLT3 and PCKLT1 glasses, as shown in Figure 3A.

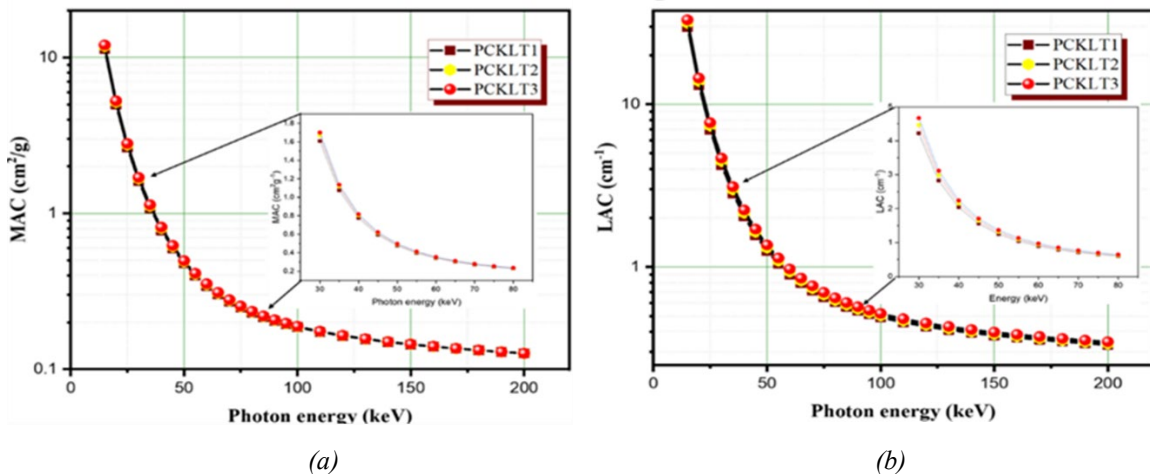


Fig. 3. (a) Mass attenuation coefficients; (b) Linear attenuation coefficients of the glasses in the energy range 15-2500KeV.

In this instance, Among the glass samples, the PCKLT3 has the greatest value of μ/ρ . while the PCKLT1 has the lowest value of μ/ρ . Consequently, the (μ/ρ) values for glasses indicated a decrease with the rise in photon energy within the specified energy range. When comparing photon shielding capabilities of different materials, the linear attenuation coefficient is one of the most important variables to consider (*LAC*). Figure 3B shows the glasses' linear attenuation coefficients when the energy level changes. With respect to the distinct photon interaction modes, the glasses' *LAC* amplitude changed with energy similarly to the *MAC*. *LAC* values likewise exhibit a similar tendency among glass types; however, the magnitude trend follows this pattern: PCKLT3 > PCKLT2 > PCKLT1. Similar to *MAC*, the highest *LAC* values

for PCKLT2 and PCKLT3 were measured at 15 KeV, with values of 31.556 and 33.013 cm^{-1} . At 20 KeV, the maximum linear attenuation coefficients for PCKLT 1, PCKLT 2, and PCKLT 3 were 13.05, 13.83, and 14.47 cm^{-1} , respectively. At 200 KeV, the smallest LAC values of 0.331668, 0.338096, and 0.34744 cm^{-1} were recorded, respectively. Using the respective findings of each glass, the remaining significant shielding parameters were then determined.

Other radiation shielding parameters such as HVL, TVL, and MFP are computed to demonstrate the calculated of radiation shielding capacity in a substance in this study [27-29]:

$$HVL = \frac{\ln(2)}{\mu} = \frac{0.693}{\mu} (\text{cm}) \quad (12)$$

$$TVL = \frac{\ln(10)}{\mu} = \frac{2.303}{\mu} (\text{cm}) \quad (13)$$

$$MFP = \frac{1}{\mu} (\text{cm}) \quad (14)$$

In the required energy range, *HVL*, *TVL*, and *MFP* have been calculated, and the results are shown in Figs. 7, 8, and 9, in order. The computed *HVL*, *TVL*, and *MFP* values for low photon energies have the lowest values, according to the figures. Then, as the energy increases, these values rise, peaking about 500 KeV. For the computed *HVL*, *TVL*, and *MFP* values in different energy areas, these differences imply that different photon interactions exist. In Figure 4A, the *HVL* values for PCKLT1, PCKLT2, and PCKLT3 samples are given, with numerical measurements of 0.023253– 2.089437 cm, 0.021961– 2.049713 cm, and 0.020991– 1.994591 cm, respectively. The *TVL* values are depicted in Figure 4B, and their numerical values are 0.077176 - 6.93464 cm, 0.072886 - 6.8028 cm, and 0.069667 - 6.619856 cm. The *MFP* are depicted in Figure 4C and their respective numerical measurements are 0.03355– 3.015061 cm, 0.03168– 2.957739 cm, and 0.03029– 2.878198 cm.

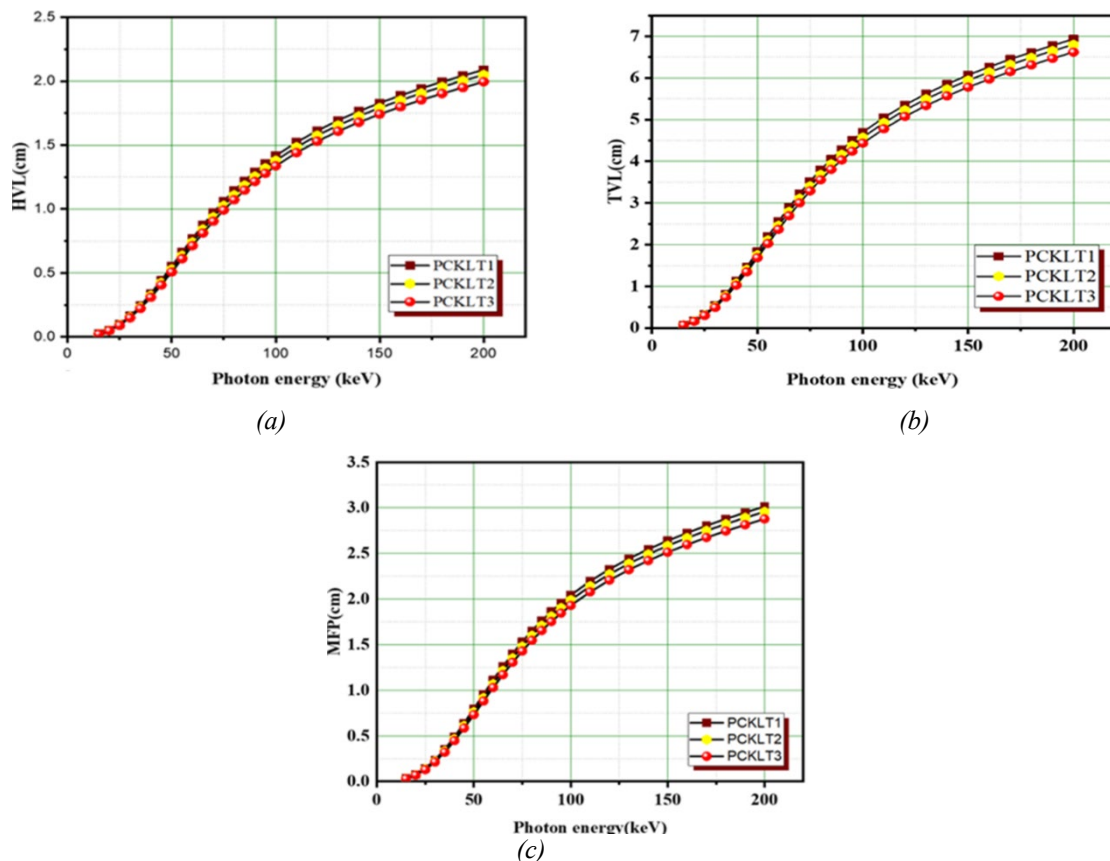


Fig.4. (a) Half value layer (HVL); (b) Tenth value layer (TVL), and (c) Mean Free Path (MFP) values of the glasses.

Comparing the results, PCKLT3 has the lowest values compared to the other glasses. Furthermore, Bioactive glass samples with the lowest HVL , TVL , and MFP values were shown to have the best X-ray radiation shielding properties.

In Eq. (15), the effective atomic number concept (Z_{eff}) can be used to describe photon interactions with the PCKLT glass system.

$$Z_{eff} = \frac{\sum i f_i A_i (\mu_m)_i}{\sum j f_j \frac{A_j}{Z_j} (\mu_m)_j} \quad (15)$$

The number of electrons per unit mass is shown by the N_{eff} . Also, N_{eff} nearly related to Z_{eff} , the N_{eff} [30] may be calculated using the equation below:

$$N_{eff} = \frac{(\mu/\rho)_c}{\sigma_e} = \frac{N_A}{M} Z_{eff} \sum i n_i (\text{electrons/g}) \quad (16)$$

These energies' Z_{eff} values were calculated in accordance with previous investigations. As seen in Figure 12, the PCKLT3 sample has the greatest Z_{eff} value, whereas the PCKLT1 sample has the smallest Z_{eff} value. The number of atoms in a material change with the energy of the radiation with which it interacts, and as a result, Z_{eff} measurements are used to determine the shielding capacity of a sample directly. When atomic numbers are high, materials with high Z_{eff} values are found, and when atomic numbers are low, materials with low Z_{eff} values are found, respectively. As a result of its lithium and titanium concentration, glass with a high Z_{eff} can be considered the best shielding material. When the Z_{eff} findings were evaluated, it was discovered that the Z_{eff} values for the three accessible Bioactive glasses were associated at the same energies. [16]. The data indicate that Z_{eff} changes with energy, and it is possible to divide the energy into photon interactions such as photoelectric, Compton, and pair production based on the investigation's findings. Also, as seen in Figure 12, the change of Z_{eff} with energy is almost the same for all glasses. Moreover, in Fig. 12, a photoelectric effect arises in the low energy region, resulting in a substantial decrease in Z_{eff} values. Also, in the middle energy region, Compton scattering is dominating, and in here, Z_{eff} has the minimum value. The process of pair production is dominating in the high energy area, and the rise from the preceding zone becomes constant there. So, the photoelectric, Compton, and pair production processes in a material are all energy dependent. [17]. As a shielding parameter, the effective electron density (N_{eff}) is of major relevance, and the values for three glasses have been computed using Eq.16. (N_{eff}) in Figure 13 changes based on photon energies such as (Z_{eff}). In all photon interactions, the variations in (Z_{eff}) and (N_{eff}) according to energy are graphically demonstrated. Analyzing Figure 13 indicates that the PCKLT3 sample has the lowest (N_{eff}) value, whereas the PCKLT1 sample has the highest (N_{eff}) value at the same energy.

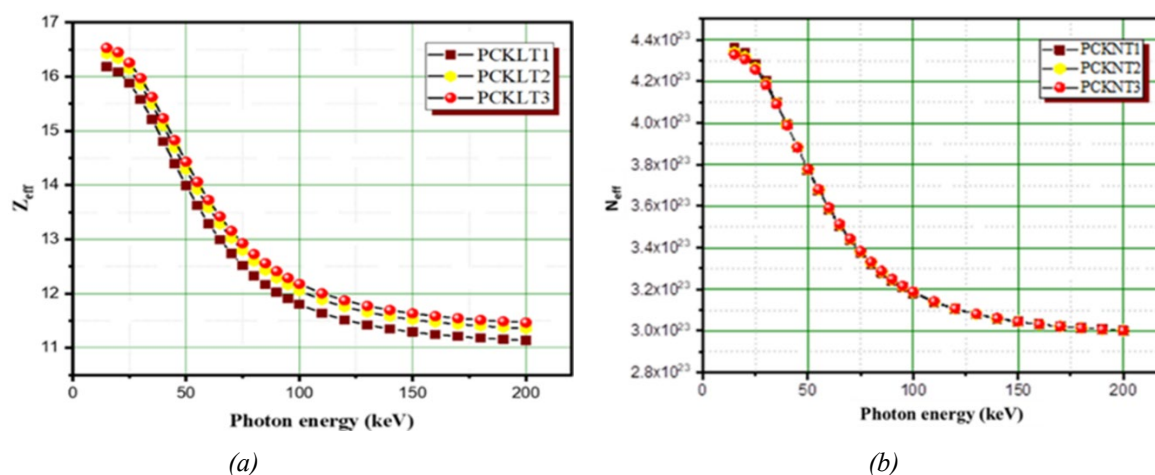


Fig. 5. (a) The effective atomic numbers, (b) The effective electron density of the prepared glasses.

3. Conclusions

The current work focuses on the structural, physical, and optical characteristics of new phosphate glasses. The density of the synthesized glasses was found to be 2.7451 g/cm^3 for PCKLT3 glass sample and decreased for sample PCKLT1. The indirect optical energy (E_{opt}) band gaps from 3.362 eV to 3.236 in Tauc's method, Urbach's energy (ΔE) changed from 0.2964 to 0.3034 . Refractive index was around ± 3 of the prepared glasses. The radiation shielding properties of recently produced bioactive glasses with a structure consisting of $45\text{P}_2\text{O}_5-20\text{CaO}-15\text{CaCl}_2-8\text{KF}-(10-x)\text{Li}_2\text{O}-2x\text{TiO}_2$ with x varying between 2 and 8 mol% were investigated. In this study, A MIKE was used to compute the μ/ρ for the glass samples under investigation over a wide range of photon energies ranging from 15 keV to 200 keV in energy. First, the mass attenuation coefficients (MAC) of the studied bioactive glasses were computed over a wide range of photon energies, as previously stated. On the basis of these MAC values, the following values were calculated: MFP , HVL , TVL , Z_{eff} , and N_{eff} . When the TiO_2 concentration was increased from 2mol% (PCKLT1 glass) to 8mol% (PCKLT3 glass), the Z_{eff} values increased from 10.98 to 11.29.

It is evident from all of the figures and tables that increasing the TiO_2 contribution in bioactive glass samples has a beneficial influence on the X-ray shielding characteristics of the materials. Furthermore, when the TiO_2 contribution to bioactive-glass samples rises, the density of the glass samples increases as well. When all of the findings are thoroughly examined, it is evident that the PCKLT3 bioactive glass sample has superior x-ray radiation attenuation capability. Our findings demonstrated that bioactive glasses doped with TiO_2 have the potential to be used in radiation shielding applications.

Acknowledgments

This work was supported by the King Khalid University through a grant RCAMS/KKU/04-22 under the Research Center for Advance Materials (RCAMS) at King Khalid University, Saudi Arabia.

References

- [1] Larry L. Hench, R. J. Splinter, W.C. Allen, T.K. Greenlee, J. Biomed. Mater. Res. 5 (6) (1971)117-141; <https://doi.org/10.1002/jbm.820050611>
- [2] Larry L. Hench, Örjan Andersson, An introduction to bioceramics (1993) 4162;

<https://doi.org/10.1142/2028>

- [3] N. Gupta, D. Santhiya, *Bioactive Glasses*, Woodhead Publishing, 2018, pp. 63-85;
<https://doi.org/10.1016/B978-0-08-100936-9.00003-4>
- [4] M.S. Al-Buriahi, V.P. Singh, *J. Australas. Ceram. Soc.* (2020) 1-7;
<https://doi.org/10.1007/s41779-020-00457-1>
- [5] Obaid, et al., *Radiat. Phys. Chem.* 144 (2018) 356-360;
<https://doi.org/10.1016/j.radphyschem.2017.09.022>
- [6] Y.S. Rammah, A.S. Abouhaswa, M.I. Sayyed, H.O. Tekin, R. El-Mallawany, *J. Non-Cryst. Solids* 509 (2019) 99-105; <https://doi.org/10.1016/j.jnoncrysol.2018.12.013>
- [7] Shamsan S. Obaid, et al., *Radiat. Eff. Defect Solid* 173 (11-12) (2018) 900-914;
<https://doi.org/10.1080/10420150.2018.1505890>
- [8] Shamsan S. Obaid, et al., *Radiat. Phys. Chem.* 148 (2018)86-94;
<https://doi.org/10.1016/j.radphyschem.2018.02.026>
- [9] O. Agar, M.I. Sayyed, F. Akman, H.O. Tekin, M.R. Kaçal, *Nucl. Eng. Technol.* 51(2019) 853-85; <https://doi.org/10.1016/j.net.2018.12.014>
- [10] M.S. Al-Buriahi, C. Sriwunkum, Halil Arslan, Baris T. Tonguc, Mohamed A. Bourham, *Appl. Phys. A* 126 (1) (2020) 1-9; <https://doi.org/10.1007/s00339-019-3254-9>
- [11] M.I. Sayyed, I.A. El-Mesady, A.S. Abouhaswa, A. Askin, Y.S. Rammah, *J. Mol. Struct.* 1197 (2019) 656-665; <https://doi.org/10.1016/j.molstruc.2019.07.100>
- [12] M.S. Al-Buriahi, Y.S. Rammah, *Appl. Phys. A* 125 (2019) 678;
<https://doi.org/10.1007/s00339-019-2976-z>
- [13] Y.Al-Hadeethi, M.I. Sayyed, Y.S. Rammah, *Int.* 46 (2020) 2055-2062;
<https://doi.org/10.1016/j.ceramint.2019.09.185>
- [14] H.O. Tekin, E. Kavaz, Athanasia Papachristodoulou, M. Kamislioglu, O. Agar, E.E. Altunsoy Guclu, O. Kilicoglu, M.I. Sayyed, *Ceram. Int.* 45 (2019) 19206-19222;
<https://doi.org/10.1016/j.ceramint.2019.06.168>
- [15] Y.Al-Hadeethi, M.I. Sayyed, *Ceram. Int.* 46 (2020) 4795-4800;
<https://doi.org/10.1016/j.ceramint.2019.10.212>
- [16] G. Susoy, EE Altunsoy Guclu, Ozge Kilicoglu, M. Kamislioglu, M.S. Al-Buriahi, M.M. Abuzaid, H.O. Tekin. *Mater. Chem. Phys.* 242 (2020) 122481;
<https://doi.org/10.1016/j.matchemphys.2019.122481>
- [17] Y. Hadeethi, M.I. Sayyed, *Ceram. Int.* 46 (2020) 6136-6140;
<https://doi.org/10.1016/j.ceramint.2019.11.078>
- [18] Y. Al-Hadeethi, M.I. Sayyed, Hiba Mohammed, Lia Rimondin, *Ceram. Int.* 46 (2020) 251-25;
<https://doi.org/10.1016/j.ceramint.2019.08.258>
- [19] H.O. Tekin, E. Kavaz, E.E. Altunsoy, O. Kilicoglu, O. Agar, T.T. Erguzel, M.I. Sayyed, *Ceram. Int.* 45 (8) (2019) 9934-9949; <https://doi.org/10.1016/j.ceramint.2019.02.036>
- [20] Ozge Kilicoglu, *Ceram. Int.* 45 (17) (2019) 23619-23631;
<https://doi.org/10.1016/j.ceramint.2019.08.073>
- [21] Ozge Kilicoglu, H.O. Tekin, *Ceram. Int.* 46 (2) (2019) 1323-1333;
<https://doi.org/10.1016/j.ceramint.2019.09.095>
- [22] Y. Al-Hadeethi, M.S. Al-Buriahi, M.I. Sayyed, *Ceram. Int.* 46 (4) (2020) 5306-5314;
<https://doi.org/10.1016/j.ceramint.2019.10.281>
- [23] Hussein, K.I.; Alqahtani, M.S.; Alzahrani, K.J.; Zahran, H.Y.; Alshehri, A.M.; Yahia, I.S.; Reben, M.; Yousef, E.S., *Crystals* 2022, 12, 941;
<https://doi.org/10.3390/cryst12070941>
- [24] J.W. Robinson, *Atomic Spectroscopy*, 2nd edn. (Taylor and Francis, Oxfordshire, 1996.
- [25] E.A. Davis, N.F. Mott, *Philos. Mag.*(1970); <https://doi.org/10.1080/14786437008221061>
- [26] R. Mirji, B. Lobo, *Radiat. Phys. Chem.* 135, 32-44 (2017);
<https://doi.org/10.1016/j.radphyschem.2017.03.001>
- [27] H.O. Tekin et al., *Mater. Chem. Phys.* 211, 9-16 (2018);

<https://doi.org/10.1016/j.matchemphys.2018.02.009>

[28] M. Sayyed et al., Mater. Chem. Phys. 217, 11-22 (2018);

<https://doi.org/10.1016/j.matchemphys.2018.06.034>

[29] H. Tekin et al., J. Non Cryst. Solids 518, 92-102 (2019);

<https://doi.org/10.1016/j.jnoncrysol.2019.05.012>

[30] J. Ngaile et al., Radiat. Prot. Dosim. 130(4), 490-498 (2008);

<https://doi.org/10.1093/rpd/ncn095>